US009281436B2

(12) **United States Patent**
Xie et al.

(10) **Patent No.: US 9,281,436 B2**
(45) **Date of Patent: Mar. 8, 2016**

(54) **RADIO-FREQUENCY SPUTTERING SYSTEM WITH ROTARY TARGET FOR FABRICATING SOLAR CELLS**

(71) Applicant: **Silevo, Inc.**, Fremont, CA (US)

(72) Inventors: **Zhigang Xie**, San Jose, CA (US); **Wei Wang**, San Jose, CA (US); **Zheng Xu**, Pleasanton, CA (US); **Jianming Fu**, Palo Alto, CA (US)

(73) Assignee: **SolarCity Corporation**, San Mateo, CA (US)

(*) Notice: Subject to any disclaimer, the term of this patent is extended or adjusted under 35 U.S.C. 154(b) by 112 days.

(21) Appl. No.: **14/142,605**

(22) Filed: **Dec. 27, 2013**

(65) **Prior Publication Data**

US 2014/0183037 A1 Jul. 3, 2014

Related U.S. Application Data

(60) Provisional application No. 61/747,081, filed on Dec. 28, 2012.

(51) **Int. Cl.**
C23C 14/34 (2006.01)
H01J 37/34 (2006.01)
(Continued)

(52) **U.S. Cl.**
CPC ***H01L 31/1876*** (2013.01); ***C23C 14/3407*** (2013.01); ***H01J 37/32082*** (2013.01); ***H01J 37/342*** (2013.01); ***H01J 37/345*** (2013.01); ***H01J 37/3405*** (2013.01); ***H01J 37/347*** (2013.01); ***H01J 37/3417*** (2013.01); ***H01J 37/3423*** (2013.01); ***H01J 37/3438*** (2013.01);
(Continued)

(58) **Field of Classification Search**
CPC . H01J 37/342; H01J 37/3452; H01J 37/3444; H01J 37/3423; H01J 37/3405; H01J 37/3417; H01J 37/3438; H01J 37/345; H01J 37/347; C23C 14/3407
USPC 204/298.21, 298.22, 192.12, 192.26
See application file for complete search history.

(56) **References Cited**

U.S. PATENT DOCUMENTS

2,626,907 A 1/1953 Melvin De Groote
2,938,938 A 5/1960 Dickson
(Continued)

FOREIGN PATENT DOCUMENTS

CN 100580957 C 1/2010
CN 104409402 3/2015
(Continued)

OTHER PUBLICATIONS

WP Leroy et al., "In Search for the Limits of Rotating Cylindrical Magnetron Sputtering", Magnetron, ION Processing and ARC Technologies European Conference, Jun. 18, 2010, pp. 1-32.
(Continued)

Primary Examiner — Rodney McDonald
(74) *Attorney, Agent, or Firm* — Shun Yao; Park, Vaughan, Fleming & Dowler LLP

(57) **ABSTRACT**

One embodiment of the present invention provides a sputtering system for large-scale fabrication of solar cells. The sputtering system includes a reaction chamber, a rotary target situated inside the reaction chamber which is capable of rotating about a longitudinal axis, and an RF power source coupled to at least one end of the rotary target to enable RF sputtering. The length of the rotary target is between 0.5 and 5 meters.

20 Claims, 5 Drawing Sheets

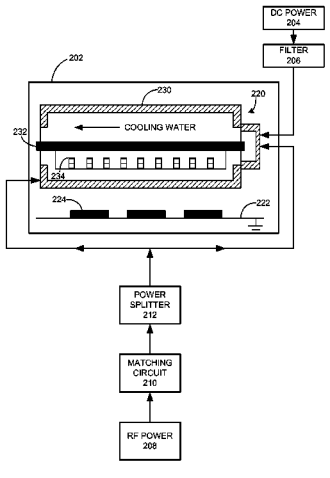

(51) **Int. Cl.**
H01L 31/18 (2006.01)
H01J 37/32 (2006.01)

(52) **U.S. Cl.**
CPC ***H01J37/3444*** (2013.01); ***H01J 37/3452*** (2013.01); ***H01L 31/1884*** (2013.01); *Y02E 10/50* (2013.01)

(56) **References Cited**

U.S. PATENT DOCUMENTS

3,094,439	A		6/1963	Mann	
3,116,171	A		12/1963	Nielson	
3,459,597	A		8/1969	Baron	
3,961,997	A		6/1976	Chu	
3,969,163	A		7/1976	Wakefield	
4,015,280	A		3/1977	Matsushita	
4,124,410	A		11/1978	Kotval	
4,124,455	A		11/1978	Lindmayer	
4,193,975	A		3/1980	Kotval	
4,200,621	A		4/1980	Liaw	
4,213,798	A		7/1980	Williams	
4,251,285	A		2/1981	Yoldas	
4,284,490	A	*	8/1981	Weber	204/298.08
4,315,096	A		2/1982	Tyan	
4,336,648	A		6/1982	Pschunder	
4,342,044	A		7/1982	Ovshinsky	
4,431,858	A		2/1984	Gonzalez	
4,514,579	A		4/1985	Hanak	
4,540,843	A		9/1985	Gochermann	
4,567,642	A		2/1986	Dilts	
4,571,448	A		2/1986	Barnett	
4,577,051	A		3/1986	Hartman	
4,586,988	A		5/1986	Nath	
4,589,191	A		5/1986	Green	
4,612,409	A		9/1986	Hamakawa	
4,633,033	A		12/1986	Nath	
4,652,693	A		3/1987	Bar-On	
4,667,060	A		5/1987	Spitzer	
4,670,096	A		6/1987	Schwirtlich	
4,694,115	A		9/1987	Lillington	
4,771,017	A		9/1988	Tobin	
4,784,702	A		11/1988	Henri	
4,877,460	A		10/1989	Flodl	
5,053,355	A		10/1991	von Campe	
5,075,763	A		12/1991	Spitzer	
5,118,361	A		6/1992	Fraas	
5,131,933	A		7/1992	Floedl	
5,178,685	A		1/1993	Borenstein	
5,181,968	A		1/1993	Nath	
5,213,628	A		5/1993	Noguchi	
5,217,539	A		6/1993	Fraas	
5,279,682	A		1/1994	Wald	
5,286,306	A		2/1994	Menezes	
5,364,518	A	*	11/1994	Hartig et al.	204/298.22
5,401,331	A		3/1995	Ciszek	
5,455,430	A		10/1995	Noguchi	
5,461,002	A		10/1995	Safir	
5,563,092	A		10/1996	Ohmi	
5,627,081	A		5/1997	Tsuo	
5,676,766	A		10/1997	Probst	
5,681,402	A		10/1997	Ichinose	
5,698,451	A		12/1997	Hanoka	
5,705,828	A		1/1998	Noguchi	
5,726,065	A		3/1998	Szlufcik	
5,814,195	A		9/1998	Lehan et al.	
5,903,382	A		5/1999	Tench	
5,935,345	A		8/1999	Kuznicki	
6,091,019	A		7/2000	Sakata	
6,140,570	A		10/2000	Kariya	
6,232,545	B1		5/2001	Samaras	
6,303,853	B1		10/2001	Fraas	
6,333,457	B1		12/2001	Mulligan	
6,441,297	B1		8/2002	Keller	
6,488,824	B1	*	12/2002	Hollars et al.	204/298.12
6,538,193	B1		3/2003	Fraas	
6,552,414	B1		4/2003	Horzel	
6,586,270	B2		7/2003	Tsuzuki	
6,620,645	B2		9/2003	Chandra	
6,683,360	B1		1/2004	Dierickx	
6,736,948	B2		5/2004	Barrett	
6,803,513	B2		10/2004	Beernink	
6,841,051	B2		1/2005	Crowley	
7,030,413	B2		4/2006	Nakamura	
7,164,150	B2		1/2007	Terakawa	
7,328,534	B2		2/2008	Dinwoodie	
7,388,146	B2		6/2008	Fraas	
7,399,385	B2		7/2008	German et al.	
7,534,632	B2		5/2009	Hu	
7,635,810	B2		12/2009	Luch	
7,737,357	B2		6/2010	Cousins	
7,749,883	B2		7/2010	Meeus	
7,769,887	B1		8/2010	Bhattacharyya	
7,772,484	B2		8/2010	Li	
7,777,128	B2		8/2010	Montello	
7,825,329	B2		11/2010	Basol	
7,829,781	B2		11/2010	Montello	
7,829,785	B2		11/2010	Basol	
7,872,192	B1		1/2011	Fraas	
7,905,995	B2		3/2011	German et al.	
8,070,925	B2		12/2011	Hoffman et al.	
8,168,880	B2		5/2012	Jacobs	
8,182,662	B2		5/2012	Crowley	
8,209,920	B2		7/2012	Krause	
8,222,513	B2		7/2012	Luch	
8,222,516	B2		7/2012	Cousins	
8,343,795	B2		1/2013	Luo	
8,586,857	B2		11/2013	Everson	
2001/0008143	A1		7/2001	Sasaoka	
2002/0086456	A1		7/2002	Cunningham	
2002/0176404	A1		11/2002	Girard	
2002/0189939	A1	*	12/2002	German et al.	204/298.12
2003/0000571	A1		1/2003	Wakuda	
2003/0042516	A1		3/2003	Forbes	
2003/0070705	A1		4/2003	Hayden	
2003/0097447	A1		5/2003	Johnston	
2003/0121228	A1		7/2003	Stoehr	
2003/0168578	A1		9/2003	Taguchi	
2003/0183270	A1		10/2003	Falk	
2003/0201007	A1		10/2003	Fraas	
2004/0065363	A1		4/2004	Fetzer	
2004/0103937	A1		6/2004	Bilyalov	
2004/0112426	A1		6/2004	Hagino	
2004/0123897	A1		7/2004	Ojima	
2004/0152326	A1		8/2004	Inomata	
2005/0012095	A1		1/2005	Niira	
2005/0022861	A1		2/2005	Rose	
2005/0064247	A1		3/2005	Sane	
2005/0109388	A1		5/2005	Murakami	
2005/0133084	A1		6/2005	Joge	
2005/0178662	A1		8/2005	Wurczinger	
2005/0189015	A1		9/2005	Rohatgi	
2005/0199279	A1		9/2005	Yoshimine	
2005/0252544	A1		11/2005	Rohatgi	
2005/0257823	A1		11/2005	Zwanenburg	
2006/0012000	A1		1/2006	Estes	
2006/0060238	A1		3/2006	Hacke	
2006/0130891	A1		6/2006	Carlson	
2006/0154389	A1		7/2006	Doan	
2006/0213548	A1		9/2006	Bachrach	
2006/0231803	A1		10/2006	Wang	
2006/0255340	A1		11/2006	Manivannan	
2006/0283496	A1		12/2006	Okamoto	
2006/0283499	A1		12/2006	Terakawa	
2007/0023081	A1		2/2007	Johnson	
2007/0023082	A1		2/2007	Manivannan	
2007/0108437	A1		5/2007	Tavkhelidze	
2007/0110975	A1		5/2007	Schneweis	
2007/0132034	A1		6/2007	Curello	
2007/0137699	A1		6/2007	Manivannan	
2007/0148336	A1		6/2007	Bachrach	
2007/0186970	A1		8/2007	Takahashi	
2007/0202029	A1		8/2007	Burns	
2007/0235829	A1		10/2007	Levine	
2007/0274504	A1		11/2007	Maes	

(56) **References Cited**

U.S. PATENT DOCUMENTS

2007/0283996	A1	12/2007	Hachtmann
2007/0283997	A1	12/2007	Hachtmann
2008/0047602	A1	2/2008	Krasnov
2008/0047604	A1	2/2008	Korevaar
2008/0092947	A1	4/2008	Lopatin
2008/0121272	A1	5/2008	Besser
2008/0121276	A1	5/2008	Lopatin
2008/0121932	A1	5/2008	Ranade
2008/0149161	A1	6/2008	Nishida
2008/0156370	A1	7/2008	Abdallah
2008/0173350	A1	7/2008	Choi
2008/0196757	A1	8/2008	Yoshimine
2008/0202577	A1	8/2008	Hieslmair
2008/0202582	A1	8/2008	Noda
2008/0216891	A1	9/2008	Harkness
2008/0230122	A1	9/2008	Terakawa
2008/0251117	A1	10/2008	Schubert
2008/0276983	A1	11/2008	Drake
2008/0283115	A1	11/2008	Fukawa
2008/0302030	A1	12/2008	Stancel
2008/0303503	A1	12/2008	Wolfs
2008/0308145	A1	12/2008	Krasnov
2009/0007965	A1	1/2009	Rohatgi
2009/0078318	A1	3/2009	Meyers
2009/0084439	A1	4/2009	Lu
2009/0101872	A1	4/2009	Young
2009/0139512	A1	6/2009	Lima
2009/0151783	A1	6/2009	Lu
2009/0155028	A1	6/2009	Boguslavskiy
2009/0188561	A1	7/2009	Aiken
2009/0221111	A1	9/2009	Frolov
2009/0239331	A1	9/2009	Xu
2009/0250108	A1	10/2009	Zhou
2009/0255574	A1	10/2009	Yu
2009/0283138	A1	11/2009	Lin
2009/0283145	A1	11/2009	Kim
2009/0293948	A1	12/2009	Tucci
2009/0320897	A1	12/2009	Shimomura
2010/0006145	A1	1/2010	Lee
2010/0015756	A1	1/2010	Weidman
2010/0043863	A1	2/2010	Wudu
2010/0065111	A1	3/2010	Fu
2010/0068890	A1	3/2010	Stockum
2010/0108134	A1	5/2010	Ravi
2010/0116325	A1	5/2010	Nikoonahad
2010/0124619	A1	5/2010	Xu
2010/0132774	A1	6/2010	Borden
2010/0132792	A1	6/2010	Kim
2010/0147364	A1	6/2010	Gonzalez
2010/0169478	A1	7/2010	Saha
2010/0186802	A1	7/2010	Borden
2010/0193014	A1	8/2010	Johnson
2010/0218799	A1	9/2010	Stefani
2010/0224230	A1	9/2010	Luch
2010/0269904	A1	10/2010	Cousins
2010/0300506	A1	12/2010	Heng
2010/0300507	A1	12/2010	Heng
2011/0146781	A1	6/2011	Laudisio
2011/0156188	A1	6/2011	Tu
2011/0168250	A1	7/2011	Lin
2011/0245957	A1	10/2011	Porthouse
2011/0259419	A1	10/2011	Hagemann
2011/0272012	A1	11/2011	Heng
2011/0277825	A1	11/2011	Fu
2011/0297227	A1	12/2011	Pysch
2012/0000502	A1	1/2012	Wiedeman
2012/0012174	A1	1/2012	Wu
2012/0028461	A1	2/2012	Ritchie et al.
2012/0031480	A1	2/2012	Tisler
2012/0040487	A1	2/2012	Asthana
2012/0085384	A1	4/2012	Beitel
2012/0125391	A1	5/2012	Pinarbasi
2012/0152349	A1	6/2012	Cao
2012/0192932	A1	8/2012	Wu
2012/0240995	A1	9/2012	Coakley
2012/0248497	A1	10/2012	Zhou
2012/0279443	A1	11/2012	Kornmeyer
2012/0279548	A1	11/2012	Munch
2012/0305060	A1	12/2012	Fu et al.
2012/0318319	A1	12/2012	Pinarbasi
2012/0318340	A1	12/2012	Heng
2012/0325282	A1	12/2012	Snow
2013/0000705	A1	1/2013	Shappir
2013/0096710	A1	4/2013	Pinarbasi
2013/0152996	A1	6/2013	DeGroot
2013/0206213	A1	8/2013	He
2013/0206221	A1	8/2013	Gannon
2013/0247955	A1	9/2013	Baba
2014/0124013	A1	5/2014	Morad
2014/0124014	A1	5/2014	Morad
2014/0196768	A1	7/2014	Heng
2014/0345674	A1	11/2014	Yang

FOREIGN PATENT DOCUMENTS

DE	4030713		4/1992
DE	102012010151		11/2013
EP	1770791		4/2007
EP	1806684		8/2007
EP	2362430		8/2011
EP	2385561	A2	11/2011
EP	2479796	A1	7/2012
EP	2626907	A1	8/2013
JP	H04245683	A	9/1992
JP	H07249788	A	9/1995
JP	2002057357	A	2/2002
JP	2005159312	A	6/2005
KR	20050122721	A	12/2005
KR	20060003277	A	1/2006
KR	20090011519	A	2/2009
WO	9117839		11/1991
WO	9120097	A1	12/1991
WO	03083953	A1	10/2003
WO	2006097189	A1	9/2006
WO	2008089657		7/2008
WO	2009150654	A2	12/2009
WO	2010075606	A1	7/2010
WO	2010104726	A2	9/2010
WO	2010123974	A1	10/2010
WO	2011005447	A2	1/2011
WO	2011008881	A2	1/2011
WO	2011053006		5/2011
WO	2011123646	A2	10/2011
WO	2013020590	A1	2/2013
WO	2010085949		3/2013
WO	2014074826		7/2014

OTHER PUBLICATIONS

Beaucarne G et al: 'Epitaxial thin-film Si solar cells' Thin Solid Films, Elsevier-Sequoia S.A. Lausanne, CH LNKD- D0I:10.1016/J.TSF.2005.12.003, vol. 511-512, Jul. 26, 2006, pp. 533-542, XP025007243 ISSN: 0040-6090 [retrieved on Jul. 26, 2006].

Chabal, Yves J. et al., 'Silicon Surface and Interface Issues for Nanoelectronics,' The Electrochemical Society Interface, Spring 2005, pp. 31-33.

Collins English Dictionary (Convex. (2000). In Collins English Dictionary. http://search.credoreference.com/content/entry/hcengdict/convex/0 on Oct. 18, 2014).

Cui, 'Chapter 7 Dopant diffusion', publically available as early as Nov. 4, 2010 at <https://web.archive.org/web/20101104143332/http://ece.uwaterloo.ca/~bcui/content/NE/%20343/Chapter/%207%20Dopant%20 diffusion%20_%201.pptx> and converted to PDF.

Davies, P.C.W., 'Quantum tunneling time,' Am. J. Phys. 73, Jan. 2005, pp. 23-27.

Dosaj V D et al: 'Single Crystal Silicon Ingot Pulled From Chemically-Upgraded Metallurgical-Grade Silicon' Conference Record of the IEEE Photovoltaic Specialists Conference, May 6, 1975, pp. 275-279, XP001050345.

Green, Martin A. et al., 'High-Efficiency Silicon Solar Cells,' IEEE Transactions on Electron Devices, vol. ED-31, No. 5, May 1984, pp. 679-683.

(56) **References Cited**

OTHER PUBLICATIONS

Hamm, Gary, Wei, Lingyum, Jacques, Dave, Development of a Plated Nickel Seed Layer for Front Side Metallization of Silicon Solar Cells, EU PVSEC Proceedings, Presented Sep. 2009.

JCS Pires, J Otubo, AFB Braga, PR Mei; The purification of metallurgical grade silicon by electron beam melting, J of Mats Process Tech 169 (2005) 16-20.

Khattak, C. P. et al., "Refining Molten Metallurgical Grade Silicon for use as Feedstock for Photovoltaic Applications", 16th E.C. Photovoltaic Solar Energy Conference, May 1-5, 2000, pp. 1282-1283.

Merriam-Webster online dictionary—"mesh". (accessed Oct. 8, 2012).

Mueller, Thomas, et al. "Application of wide-band gap hydrogenated amorphous silicon oxide layers to heterojunction solar cells for high quality passivation." Photovoltaic Specialists Conference, 2008. PVSC'08. 33rd IEEE. IEEE, 2008.

Mueller, Thomas, et al. "High quality passivation for heteroj unction solar cells by hydrogenated amorphous silicon suboxide films." Applied Physics Letters 92.3 (2008): 033504-033504.

Munzer, K.A. "High Throughput Industrial In-Line Boron BSF Diffusion" Jun. 2005. 20th European Photovoltaic Solar Energy Conference, pp. 777-780.

National Weather Service Weather Forecast Office ("Why Do We have Seasons?" http://www.crh.noaa.gov/lmk/?n=seasons Accessed Oct. 18, 2014).

O'Mara, W.C.; Herring, R.B.; Hunt L.P. (1990). Handbook of Semiconductor Silicon Technology. William Andrew Publishing/Noyes. pp. 275-293.

Roedern, B. von, et al., 'Why is the Open-Circuit Voltage of Crystalline Si Solar Cells so Critically Dependent on Emitter-and Base-Doping?' Presented at the 9th Workshop on Crystalline Silicon Solar Cell Materials and Processes, Breckenridge, CO, Aug. 9-11, 1999.

Stangl et al., Amorphous/Crystalline Silicon heterojunction solar cells—a simulation study; 17th European Photovoltaic Conference, Munich, Oct. 2001.

Warabisako T et al: 'Efficient Solar Cells From Metallurgical-Grade Silicon' Japanese Journal of Applied Physics, Japan Society of Applied Physics, JP, vol. 19, No. SUPPL. 19-01, Jan. 1, 1980, pp. 539-544, XP008036363 ISSN: 0021-4922.

Yao Wen-Jie et al: 'Interdisciplinary Physics and Related Areas of Science and Technology;The p recombination layer in tunnel junctions for micromorph tandem solar cells', Chinese Physics B, Chinese Physics B, Bristol GB, vol. 20, No. 7, Jul. 26, 2011, p. 78402, XP020207379, ISSN: 1674-1056, DOI: 10.1088/1674-1056/20/7/078402.

* cited by examiner

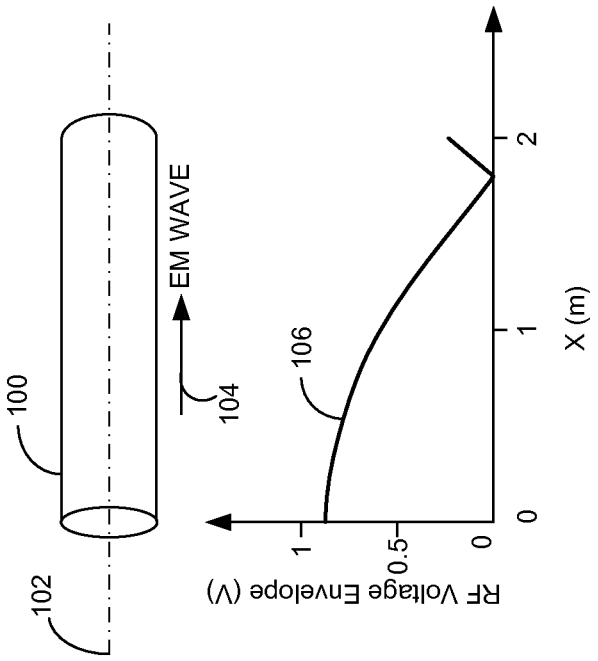

FIG. 1

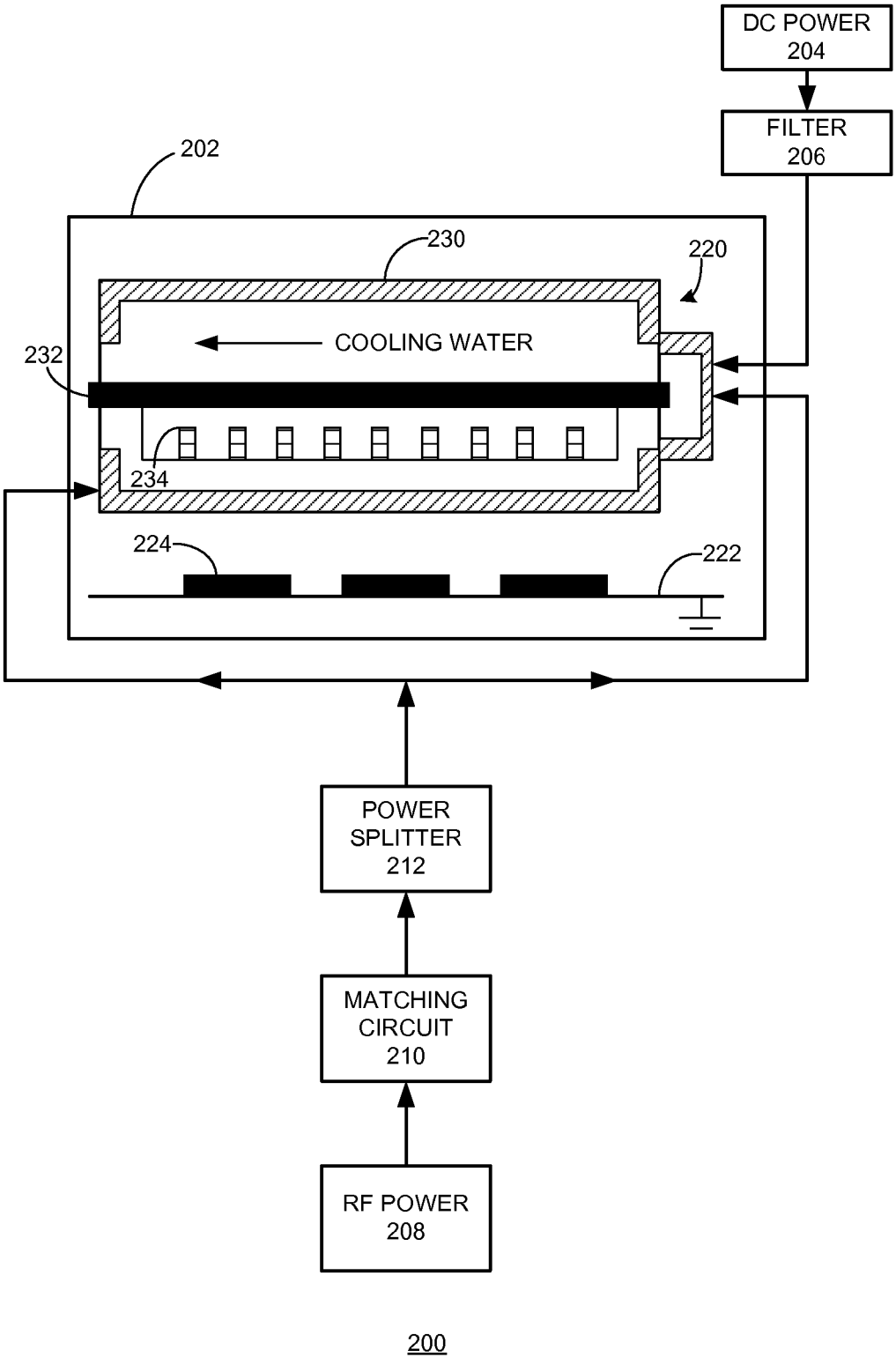
DC POWER
204
FILTER
206
202
230
220
COOLING WATER
232
234
224
222
POWER
SPLITTER
212
MATCHING
CIRCUIT
210
RF POWER
208
200

FIG. 2

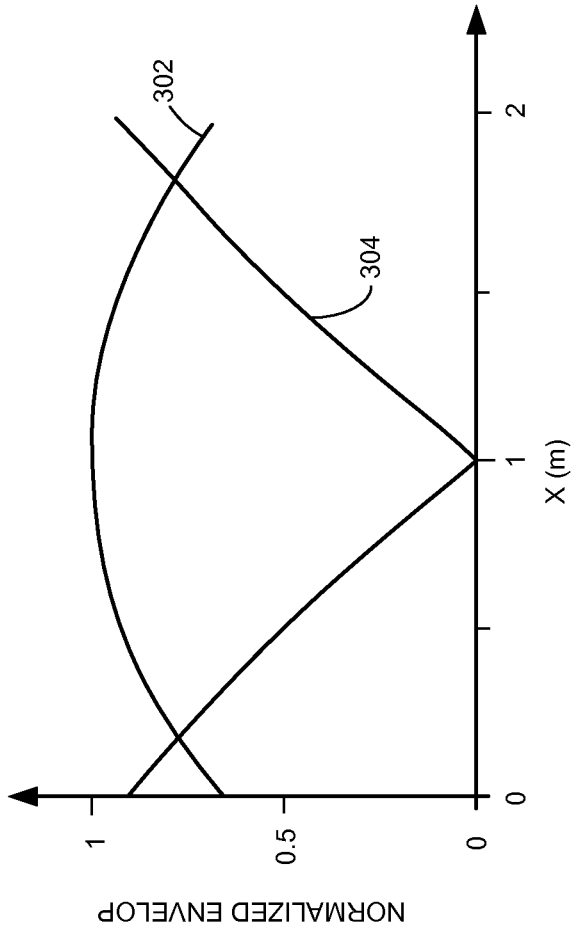

FIG. 3

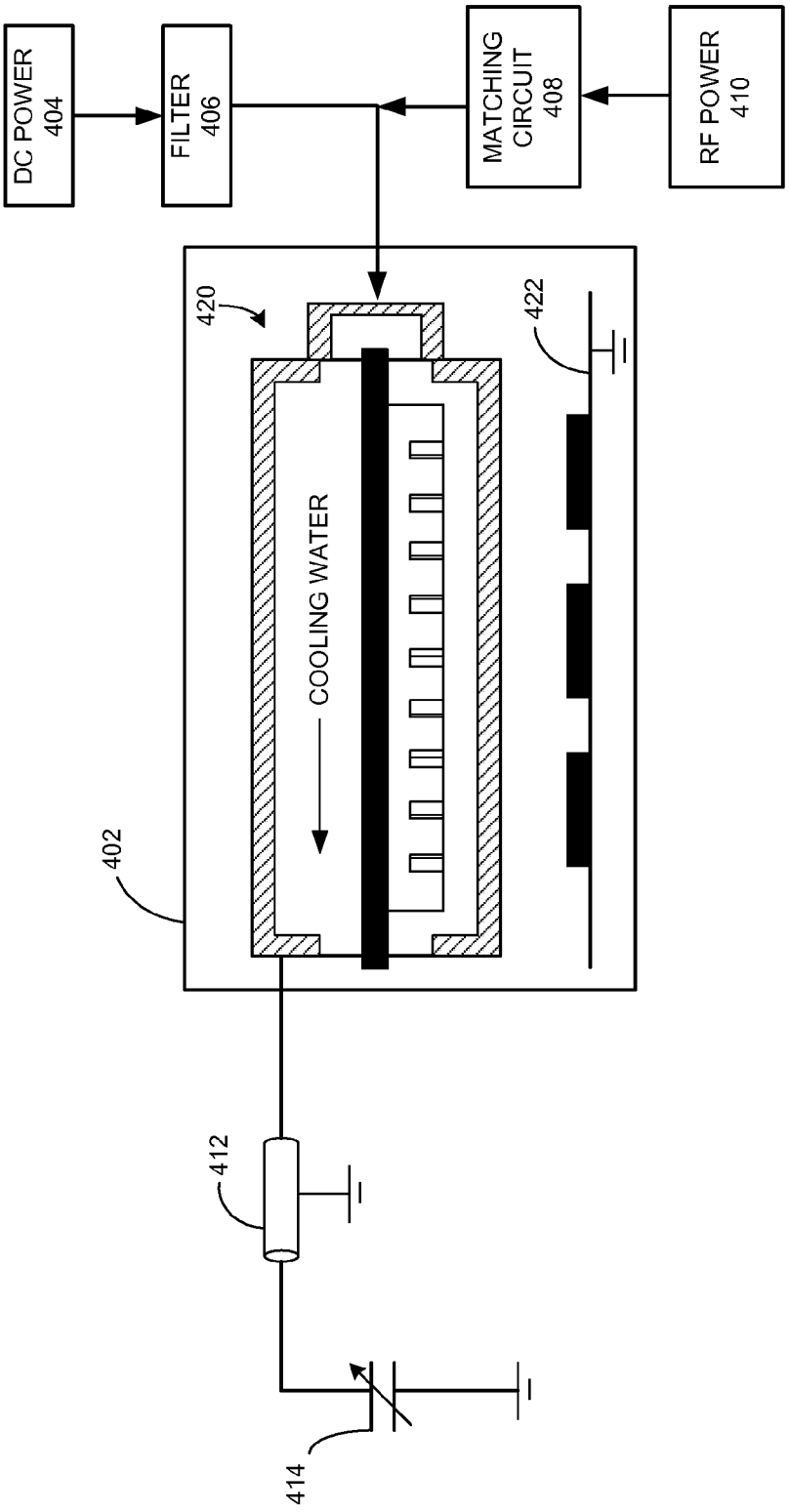
DC POWER
404
FILTER
406
MATCHING
CIRCUIT
408
RF POWER
410
420
422
COOLING WATER
402
412
414
400

FIG. 4

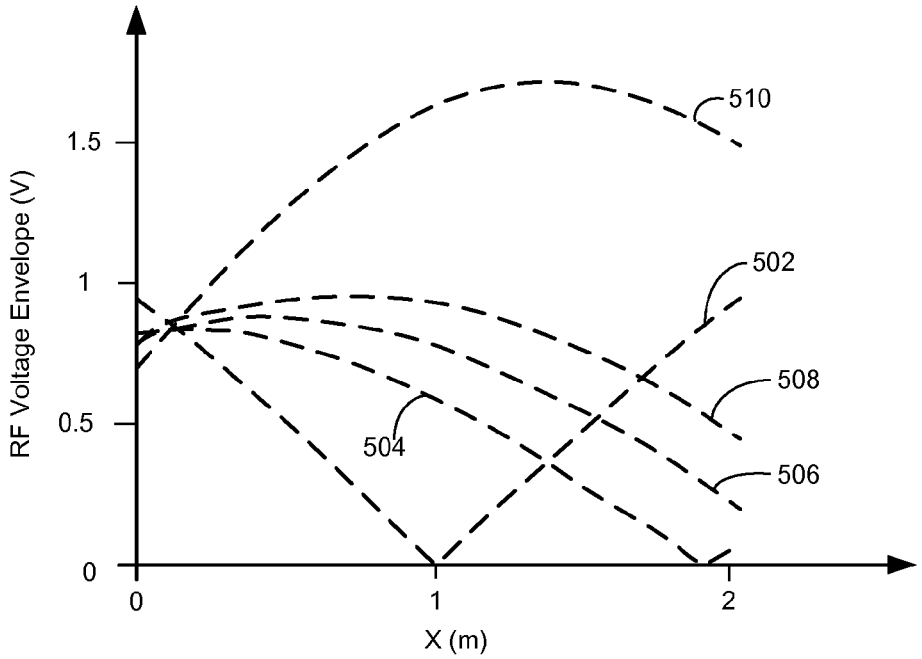
RF Voltage Envelope (V)
1.5
1
0.5
0
0
1
2
X (m)
510
502
508
506
504

FIG. 5

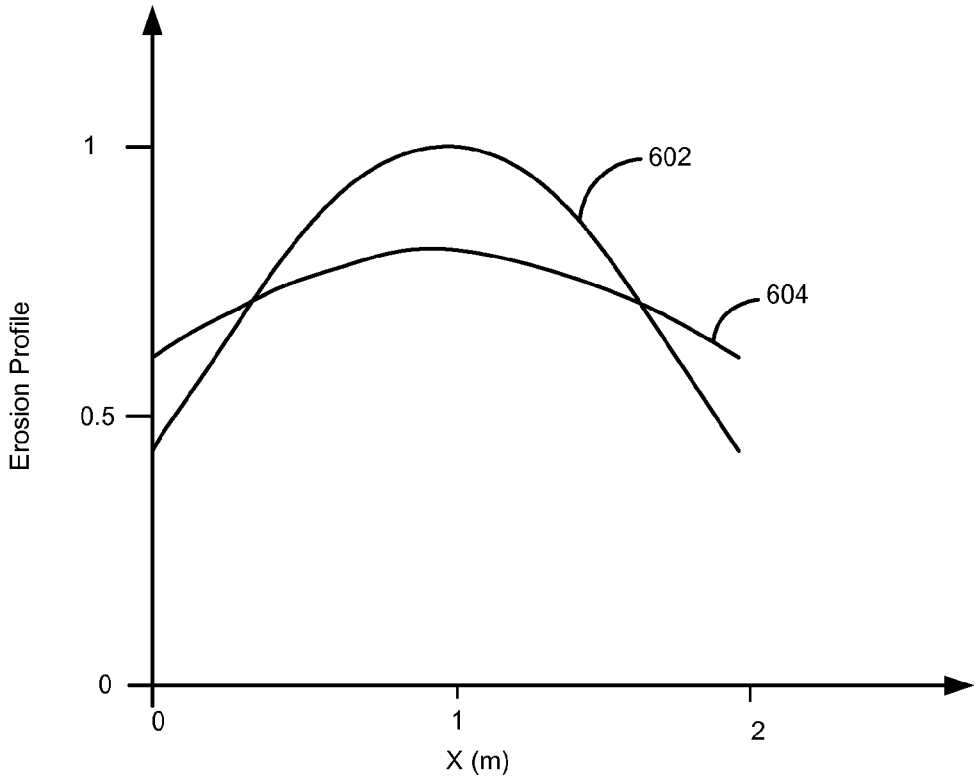
Erosion Profile
1
0.5
0
0
1
2
X (m)
602
604

FIG. 6

RADIO-FREQUENCY SPUTTERING SYSTEM WITH ROTARY TARGET FOR FABRICATING SOLAR CELLS

RELATED APPLICATION

This application claims the benefit of U.S. Provisional Application No. 61/747,081, entitled "Applying Radio-Frequency Sputtering to a Rotary Target System," by inventors Zhigang Xie, Wei Wang, Zheng Xu, and Jianming Fu, filed 28 Dec. 2012.

BACKGROUND

1. Field

This disclosure is generally related to a sputtering system used for fabricating solar cells. More specifically, this disclosure is related to a radio frequency (RF) sputtering system equipped with a rotary target.

2. Related Art

Anti-reflection coatings (ARCs) play an important role in ensuring high efficiency of silicon-based solar cells because the bare Si has a high surface reflection rate. Most ARCs include one or more layers of dielectrical material, such as SiO_2, SiN_x, etc. Moreover, many solar cells also include a thin layer of transparent conducting oxide (TCO) material (such as indium-tin-oxide (ITO) or indium doped zinc oxide (ZIO)), which may also act as an ARC layer, on their top surface to ensure good ohmic contact between the metal electrode and the underlying Si layers.

Among various film deposition techniques, sputtering has been widely used by solar cell manufacturers as a tool for depositing the ARC and/or TCO layers because it can provide a high-quality film with sufficiently low interface defect density (D_{it}), which is important for achieving high-efficiency solar cells. However, currently available sputtering systems for manufacturing PVDs often rely on applying a high direct-current (DC) voltage to the target, and may result in a charge build-up on floating-potential surfaces and arcing. The occurrence of arcing makes the plasma and the deposition process unstable and therefore unpredictable. To decrease the influence of the arcing effect, alternating voltages can be used to prevent charge build-up at the floating-potential surface. However, DC-pulsed sputtering usually cannot meet the low-damage requirement of high-efficiency solar cells.

SUMMARY

One embodiment of the present invention provides a sputtering system for large-scale fabrication of solar cells. The sputtering system includes a reaction chamber, a rotary target situated inside the reaction chamber which is capable of rotating about a longitudinal axis, and an RF power source coupled to at least one end of the rotary target to enable RF sputtering. The length of the rotary target is between 0.5 and 5 meters.

In a variation on the embodiment, the system further includes a power splitter coupled to the RF power source. The RF splitter is configured to split output of the RF power source into two portions and feed each of the two portions to one end of the rotary target.

In a further variation, the power splitter is configured to split the output of the RF source 50-50.

In a variation on the embodiment, the system further includes a plurality of magnets configured to generate a static magnetic field between the rotary target and a carrier that carries a plurality of solar cells.

In a further variation, the RF power source has an RF frequency of at least 13 MHz.

In a variation on the embodiment, the system further includes a capacitance tuner coupled to one end of the rotary target.

In a further variation, the system further includes a tuning mechanism configured to periodically tune the capacitance tuner over a predetermined capacitance range.

In a further variation, the predetermined capacitance range is between 0.5 nF and 50 nF.

In a further variation, the system further includes a coaxial cable configured to couple the capacitance tuner with one end of the rotary target.

In a variation on the embodiment, the rotary target includes one or more layers of ceramic materials. The ceramic materials include one or more of: a transparent conducting oxide (TCO) material and a dielectric material.

BRIEF DESCRIPTION OF THE FIGURES

FIG. **1** presents a diagram illustrating an exemplary rotary target and a voltage distribution profile for across the rotary target under the condition of RF sputtering.

FIG. **2** presents an exemplary magnetron RF sputtering system with a rotary target, in accordance with an embodiment of the present invention.

FIG. **3** presents a diagram illustrating exemplary voltage and current distribution profiles of a rotary target along its longitudinal axis during RF sputtering, in accordance with an embodiment of the present invention.

FIG. **4** presents a diagram illustrating an exemplary magnetron RF sputtering system with a rotary target, in accordance with an embodiment of the present invention.

FIG. **5** presents a diagram illustrating the voltage profiles of the rotary target when the capacitance tuner is tuned to different capacitances, in accordance with an embodiment of the present invention.

FIG. **6** presents a diagram illustrating exemplary target erosion profiles for different RF sputtering systems, in accordance with an embodiment of the present invention.

In the figures, like reference numerals refer to the same figure elements.

DETAILED DESCRIPTION

The following description is presented to enable any person skilled in the art to make and use the embodiments, and is provided in the context of a particular application and its requirements. Various modifications to the disclosed embodiments will be readily apparent to those skilled in the art, and the general principles defined herein may be applied to other embodiments and applications without departing from the spirit and scope of the present disclosure. Thus, the present invention is not limited to the embodiments shown, but is to be accorded the widest scope consistent with the principles and features disclosed herein.

Overview

Embodiments of the present invention provide an RF sputtering system equipped with a rotary target to ensure uniform film deposition and target erosion. To prevent a formation of a standing wave, in some embodiments, the RF power is split 50-50 and each portion is fed to one end of the rotary target. In alternative embodiments, one end of the rotary target is coupled to the RF power, and the other end is coupled to a capacitance tuner. By periodically tuning the capacitance tuner, one can achieve a relatively flat profile of the average voltage across the rotary target. A flat voltage profile ensures

uniform target erosion. In further embodiments, increasing magnetic pole density at the plasma edge can further balance the erosion profile along the axis of the rotary target.

Electro-magnetic Field Distribution

Industrialized fabrications of solar cells often involve a relatively large film-deposition system. Some systems can include an inline feeding mechanism that feeds a wafer carrier that carries multiple solar cell wafers arranged into an m×n array into a deposition chamber. As the wafers pass through beneath (sometime above) the target, a thin layer of target material is deposited onto the wafer surface via reactive sputtering. For large-scale deposition, the size of the chamber can be up to a few meters long and over a meter wide. The size of a typical target used in such chambers can also be a few meters long.

Conventional sputtering systems often use planar targets that are often eroded non-uniformly in the sputter chamber and have a low target-utilization rate of around 30%. Moreover, when insulation targets, such as ceramic AZO targets are used, nodule formation and excessive arcing may occur, which further degrades target utilization and film quality. To prolong the target life and to reduce maintenance costs (switching out a target requires an interruption of the inline deposition process), sputtering systems with rotary targets have been used in large-scale solar cell fabrications.

When magnetron power is used during sputtering to confine the plasma, the use of a rotary target can also result in a cooler target because the magnetron power is spread out over a larger area in a given amount of time as the target is rotating continuously. Additional approaches used to reduce the nodule formation and occurrences of arcing also include usages of pulsed-DC power or AC (alternating current) power. However, pulsed-DC or AC sputtering often cannot provide a low-enough D_{it} desirable for high-efficiency solar cells.

In order to obtain thin films with a low D_{it}, to prolong target lifetime, and to reduce maintenance costs (or the cost of ownership), in some embodiments, the sputtering system incorporates radio-frequency (RF) sputtering with a rotary target.

To apply RF sputtering, the rotary target is coupled to an RF power source; electromagnetic waves at the RF band travel along the axis of the rotary target and are confined between the surface of the target and the plasma body. A standard rotary target can be a cylindrical tube that is a few meters in length and 10-20 centimeters in diameter. Due to the boundary conditions, the transverse electromagnetic (TEM) mode is the only allowed propagating mode, with the electrical field (the E-field) in a direction normal to the target surface and the magnetic field (the B-field) in a direction tangential to the target surface. This oscillating electromagnetic field, along with the static magnetic field generated by the magnets, creates and maintains the collision and ionization, and the spiral motion of electrons.

Typical frequencies used for RF sputtering are around tens of MHz, such as 13.56 MHz or 40 MHz, meaning the wavelength of the electromagnetic wave can range from a few meters (for higher frequency) to a few tens of meters (for lower frequency). Note that as the wavelength of the electromagnetic wave becomes comparable with the length of the rotary target, standing waves can form, which can then result in uneven sputtering, with the most sputtering at the anti-node and the least sputtering at the node of the standing wave. Such a sputtering pattern is determined by the voltage profile across the rotary target. In general, more target erosion occurs at points with a higher voltage. FIG. **1** presents a diagram illustrating an exemplary rotary target and a voltage distribution profile for across the rotary target under the condition of RF sputtering.

In FIG. **1**, a rotary target **100** includes a cylinder that is capable of rotating about a longitudinal axis **102**. Note that for the deposition of TCO materials, rotary target **100** may be a ceramic target with metal backings. Arrow **104** indicates the propagating direction of the electromagnetic wave. In the example shown in FIG. **1**, the length of rotary target **100** is about 2 meters, and curve **106** indicates the voltage envelope along the longitudinal axis of target **100**. In this example, an RF power source is coupled to one end of rotary target **100**. As one can see from FIG. **1**, the voltage distribution along longitudinal axis **102** is not uniform; node (where the voltage is zero) or anti-node (where the voltage is maximum) may exist, meaning that certain points may experience heavy erosion whereas a different point may experience lighter erosion. Note that such an uneven erosion profile can be problematic for continuous sputtering because the target cannot be effectively utilized. In addition, the non-uniform voltage profile can also result in a non-uniform film deposition.

A good sputtering system requires that the localized erosion rate should be more than the re-deposition rate in order to reduce particle contamination. This means that the sputtering system should have a node-less voltage profile along the longitudinal axis. To do so, in some embodiments, an RF sputtering system includes RF feeds coupled to both ends of the rotary target to eliminate the node in the voltage distribution profile.

FIG. **2** presents an exemplary magnetron RF sputtering system with a rotary target, in accordance with an embodiment of the present invention. In FIG. **2**, RF sputtering system **200** includes a reactor chamber **202**, a DC power source **204**, a filter **206**, an RF power source **208**, an RF matching circuit **210**, and a power splitter **212**. Within reactor chamber **202** there is a rotary target **220** and a carrier **222**. More specifically, rotary target **220** includes a cylindrical tube **230** capable of rotating about a longitudinal axis **232**. In some embodiments, cylindrical tube **230** includes a metal backing tube (as indicated by the shaded areas) coated with ceramic powders. In some embodiments, cylindrical tube **230** includes one or more ceramic layers (with a thickness of up to a few centimeters) bonded to a metal backing tube. Note that the metal backing tube not only provides support to the ceramic layers but also acts as a conductor and a waveguide for the electromagnetic waves. The length of cylindrical tube **230** can be between 0.5 and 5 meters. In some embodiments, cylindrical tube **230** has a length between 2 and 3 meters. A number of stationary magnets, such as a stationary magnet **234**, are mounted to longitudinal axis **232**. These stationary magnets provide a stationary magnetic field, which confines the plasma in front of rotary target **220**. To reduce heating, cooling water flows within cylindrical tube **230**. In the example shown in FIG. **2**, a carrier (also known as a pallet) **222**, which carries a number of solar cells (such as a solar cell **224**) for deposition, is placed beneath rotary target **220**, and longitudinal axis **232** is parallel to the surface of carrier **222**. In practice, the relative positions between rotary target **220** and carrier **222** can be different. In some embodiments, rotary target **220** may be placed in a position such that longitudinal axis **232** is vertical to the surface of carrier **222**. Note that other standard components (such as a rotation mechanism that rotates the target continuously, load locks, and a gas delivery system) that are included in a sputtering system are not shown in FIG. **2**.

DC power source **204** is coupled to one end of rotary target **220** via filter **206** to provide a static electrical field between

rotary target **220** and grounded (or floating) carrier **222**. Filter **206** acts as an AC blocker that blocks possible AC power leakage back to DC power source **204**. RF power source **208** is coupled to both ends of rotary target **220** via matching circuit **210** and power splitter **212**. Note that matching circuit **210** provides impedance matching between RF power source **208** and rotary target **220**. Such matching is needed to provide maximum power transfer and to reduce RF reflection. In some embodiments, matching circuit **210** can include matching networks, such as a Pi matching network, a T matching network, and an L matching network.

Power splitter **212** splits the RF power into two separate portions and feeds each portion to one end of rotary target **220**. In some embodiments, power splitter **212** splits the RF power 50-50, and the evenly split power is fed to both ends of rotary target **220**. More specifically, each output of power splitter **212** is electrically coupled to one end of the metal tube included in cylindrical tube **230**. Here, the metal tube acts as a waveguide for the RF wave, and the same power feeding at each end of the metal tube results in a symmetrical boundary condition for the waveguide. Note that assuming TEM mode is the only allowed propagation mode in the waveguide, the RF energy flux is transferred back and forth in the direction along longitudinal axis **232**. One can model this distributed system to include a resistance (due to the skin effect in the RF regime) across rotary target **220**, an inductance (due to the current flow in the direction along longitudinal axis **232**), a conductance across the plasma sheath, and an effective capacitance between the surface of rotary target **220** and the plasma. Note that due to the magnetic field, the plasma is confined between rotary target **220** and carrier **222**. In this modeling, voltage profile along longitudinal axis **232** is proportional to the vertical electrical field across the plasma sheath, and hence is more relevant to the ionization and local target erosion. In other words, a higher voltage means more target erosion. On the other hand, electrons follow a spiral motion primarily defined by the static magnetic field. Due to considerable scattering effects, the erosion groove can be smoothed out.

Based on the aforementioned model and the boundary condition (which is symmetrical if power splitter **212** is a 50-50 splitter), one can calculate the voltage and current distribution on rotary target **220** along its longitudinal axis **232**. FIG. **3** presents a diagram illustrating exemplary voltage and current distribution profiles of a rotary target along its longitudinal axis during RF sputtering, in accordance with an embodiment of the present invention. In FIG. **3**, curve **302** and curve **304** indicate the voltage and current profile across the rotary target, respectively. In the example shown in FIG. **3**, the length of the rotary target is around 2 meters and the frequency of the RF power is assumed to be 40 MHz. Moreover, it is assumed that a power splitter evenly splits the RF power and feeds an equal portion to each end of the rotary target. As one can see from FIG. **3**, the symmetrical boundary condition results in a symmetrical voltage and current distribution, with the voltage profile having an anti-node and the current profile having a node right in the middle of the rotary target. Note that by adjusting the power-splitting ratio and phase, one can move the locations of the anti-node and the node. Comparing FIG. **3** with FIG. **1**, one can see that by feeding the RF power from both ends of the rotary target, one can remove the node in the voltage profile and obtain a more uniform voltage distribution. Such a relative uniform voltage profile across the rotary target is important for achieving relatively even erosion across the target. Consequently, the film deposition can be more uniform, and the target utilization can be increased.

In general, RF sputtering system **200** shown in FIG. **2** works well with RF powers at a lower frequency, such as the commonly used 13.56 MHz. However, to achieve thin films with D_{it} matching the requirements of high-efficiency solar cells, RF powers at a higher frequency, such as 40 MHz or higher, are needed. At such a high frequency, the RF wavelength is very close to the length of the rotary target, meaning that considerable phase shifts exist on the rotary target from one end to the other, and thus, a considerable change in voltages across the target. As one can see in FIG. **3**, although improved, the voltage profile (curve **302**) still shows that the voltage at the center of the rotary target is significantly higher than the voltage at the end of the rotary target. In some embodiments, the stationary magnets are rearranged such that a stronger magnetic field can be achieved at the edge of the rotary target in order to even out the voltage profile. For example, one can increase the density of the magnets at locations closer to the edge of the rotary target. However, effects of such improvements can be limited and a better solution is still needed for higher frequency RF sputtering.

To further improve the uniformity of the voltage distribution, especially in cases of higher frequency RF sputtering, in some embodiments, the RF sputtering system includes a capacitance tuner coupled to one end of the rotary target. By tuning the capacitance tuner over a certain range and averaging the overall effects, one can achieve a more uniform voltage profile along the longitudinal axis of the rotary target. FIG. **4** presents a diagram illustrating an exemplary magnetron RF sputtering system with a rotary target, in accordance with an embodiment of the present invention.

In FIG. **4**, RF sputtering system **400** includes a reactor chamber **402**, a DC power source **404**, a filter **406**, a matching circuit **408**, an RF power source **410**, a piece of coaxial cable **412**, and a capacitance tuner **414**. Similar to reactor chamber **202** shown in FIG. **2**, reactor chamber **402** includes a rotary target **420** and a carrier **422**. Rotary target **420** includes a cylindrical tube capable of rotating about its longitudinal axis, and a number of stationary magnets mounted on the longitudinal axis. To reduce the heating of the target, cooling water flows inside the cylindrical tube. Note that the cylindrical tube can include a metal backing tube and one or more ceramic layers on the surface of the metal tube. In some embodiments, the ceramic layers can include common TCO materials, such as ITO and IZO, and dielectric materials, such as SiO_2. The length of rotary target **420** can be between 0.5 and 5 meters. In some embodiments, rotary target **420** has a length of at least 2 meters to enable large-scale operations that are required in the manufacturing of solar cells. Moreover, carrier **422** is capable of carrying multiple solar cells for simultaneous film deposition on these cells.

Similar to the sputtering system shown in FIG. **2**, DC power source **404** is coupled to one end of rotary target **420** (more specifically, electrically coupled to the metal backing tube) via filter **406** to provide a static electrical field between rotary target **420** and grounded carrier **422**. Filter **406** acts as an AC blocker that blocks possible AC power leakage back to DC power source **404**. Unlike the system shown in FIG. **2**, in FIG. **4**, RF power source **410** is coupled to only one end of rotary target **420** via matching circuit **408**. In some embodiments, a single electrode can be used to couple rotary target **420** with DC power source **404** and RF power source **410**.

The other end of rotary target **420** is coupled to capacitance tuner **414** via coaxial cable **412**. Note that the grounded capacitance tuner **414** together with coaxial cable **412** can partially reflect electromagnetic wave, and create a tunable boundary condition. Note that the length and characteristics of coaxial cable **412** is carefully chosen to match the charac-

teristic impedance of the target for TEM propagation in order to avoid unnecessary loss of RF energy. In one embodiment, coaxial cable **412** has a characteristic impedance of 50 ohm and is 10.2 feet long. By tuning the capacitance of capacitance tuner **414**, one can move the location of the node (or anti-node) from one side of the rotary target to the other side of the rotary target, assuming linear tuning. FIG. **5** presents a diagram illustrating the voltage profiles of the rotary target when the capacitance tuner is tuned to different capacitances, in accordance with an embodiment of the present invention. In the example shown in FIG. **5**, the length of the rotary target is approximately 2 meters, and the RF frequency is set at 40 MHz. Curve **502** represents the voltage distribution along the longitudinal axis of the rotary target when the capacitance tuner is tuned to 1.2 nF, and curves **504**, **506**, **508**, and **510** are obtained when the capacitance tuner is tuned to 1.6 nF, 1.8 nF, 2 nF, and 4 nF, respectively. As one can see from FIG. **5**, when the capacitance tuner is set at 1.2 nF, a node exists in the voltage profile approximately at the center of the rotary target. As the capacitance that is coupled to one end of the rotary target increases, the location of the node moves. For example, when the capacitance tuner is set at 1.6 nF, the voltage node moves to a location that is closer to an edge of the rotary target. Similarly, the location of the voltage anti-node also moves when the capacitance changes. Hence, by carefully tuning the capacitance tuner, we might be able to obtain a voltage profile that is relatively flat. For example, in FIG. **5**, curve **508** may provide the most flat voltage distribution compared with other curves shown in FIG. **5**. Moreover, by carefully arranging the magnets, one can further improve the voltage distribution uniformity, which is essential in obtaining a more uniform erosion profile.

Considering that the effect of target erosion takes time, one can obtain a more uniform voltage profile by averaging over time the different voltage profiles shown in FIG. **5**. To do so, one can tune the capacitance tuner periodically. As long as the tuning period is much shorter compared with the deposition time (or the tuning frequency is much lower than the feeding speed of the inline sputtering system), the overall etching of the target during the deposition is averaged over the various settings of the capacitance tuner. In some embodiments, the capacitance tuner has a tuning range from 0.5 nF up to 50 nF (such as ranging from 1.2 nF to 4 nF), and the tuning frequency can range from a few Hz to a few tens of Hz. Depending on the configuration of the capacitance tuner, various methods can be used to periodically tune the capacitance tuner. In some embodiments, the capacitance tuner includes a mechanically controlled variable capacitor, such as a rotary variable capacitor, whose capacitance can be tuned by tuning the distance between the plates of the amount of overlapping plate surface areas. For example, the rotary variable capacitor can be coupled to a rotary motor. The constant rotation of the rotary motor periodically tunes the capacitance of the variable capacitor, and the tuning frequency can be determined by the speed of the rotary motor. In some embodiments, in addition to a capacitance tuner, the tunable boundary condition can also be provided by a tunable resistor, a tunable inductor, or a combination thereof. For example, a capacitance tuner can be coupled to a resistor, either in series or in parallel, to provide the needed tunable boundary condition.

FIG. **6** presents a diagram illustrating exemplary target erosion profiles for different RF sputtering systems, in accordance with an embodiment of the present invention. Note that the erosion profile is proportional to the RF energy profile along the longitudinal axis of the rotary target. In FIG. **6**, the RF frequency is approximately 40 MHz, and the target length is approximately 2 meters. Curve **602** indicates the target erosion profile for an RF sputtering system with fixed, symmetrical boundary conditions, such as the RF sputtering system shown in FIG. **2**. Curve **604** indicates the target erosion profile of an RF sputtering system with continuously tuned boundary conditions, such as the RF sputtering system shown in FIG. **4**. As one can see, with the continuously tuned boundary condition, the time-averaged erosion profile is much more uniform compared with the fixed, symmetrical boundary condition. In the example shown in FIG. **6**, the capacitance tuner is tuned between 1.2 nf and 4 nf, and the coaxial cable has a characteristic impedance of 50 ohm and a length of 10.2 ft. Different erosion profiles can be obtained if these parameters are changed.

As one can see, even with the continuously tuned boundary condition, more erosion still occurs at the center of the target than at the edges. Such non-uniformity can be corrected by rearranging the stationary magnets as the erosion profile is also dependent on the magnetic field. In some embodiments, the stationary magnets may include an array of ferromagnetic pole pieces that are mechanically mounted to the longitudinal axis of the rotary target. Hence, by rearranging the magnets to have a higher density of pole pieces at both edges of the rotary target, we can further improve the target erosion uniformity.

Note that FIGS. **2** and **4** are merely schematic views of exemplary sputtering systems. Certain system components, such as rotation motors and wafer loading mechanisms, are not shown in FIGS. **2** and **4**. Moreover, in practice, the shape and size of the chamber and chamber components, such as the rotary target and the magnets, can be different than the ones shown in FIGS. **2** and **4**. In FIG. **4**, the capacitance tuner is coupled to the end of the rotary target that is not coupled to the RF source. In practice, it is also possible to combine FIGS. **2** and **4** so that both ends of the rotary target are coupled to an RF power source, and at least one end of the rotary target is coupled to a capacitance tuner. As long as the rotary target has periodically tuned boundary conditions, it is possible to obtain a relatively uniform erosion profile because the time average of the voltage distributions is relatively flat. Note that the boundary conditions, which are determined by the tuning range of the capacitance tuner and the amount of RF power fed at each end, can be selected carefully to obtain the optimal erosion uniformity.

The foregoing descriptions of various embodiments have been presented only for purposes of illustration and description. They are not intended to be exhaustive or to limit the present invention to the forms disclosed. Accordingly, many modifications and variations will be apparent to practitioners skilled in the art. Additionally, the above disclosure is not intended to limit the present invention.

What is claimed is:

1. A sputtering system for large-scale fabrication of solar cells, comprising:

a reaction chamber;

a rotary target situated inside the reaction chamber, wherein the rotary target is configured to rotate about a longitudinal axis; and

an RF power source coupled to the rotary target to enable RF sputtering, wherein a length of the rotary target is between 0.5 and 5 meters, wherein output of the RF power source is divided into two portions, and wherein each of the two portions is sent to one end of the rotary target.

2. The sputtering system of claim **1**, wherein the output of the RF source is split into two equal portions.

3. The sputtering system of claim 1, further comprising a plurality of magnets configured to generate a static magnetic field between the rotary target and a carrier that carries a plurality of solar cells.

4. The sputtering system of claim 2, wherein the plurality of magnets are arranged in such a way that magnetic field is stronger at a location corresponding to an edge of the rotary target, thereby facilitating the magnetic field to have a higher strength at the edge of the rotary target.

5. The sputtering system of claim 1, wherein the RF power source has an RF frequency of at least 13 MHz.

6. The sputtering system of claim 1, further comprising a capacitance tuner coupled to one end of the rotary target.

7. The sputtering system of claim 6, further comprising a tuning mechanism configured to periodically tune the capacitance tuner over a predetermined capacitance range.

8. The sputtering system of claim 7, wherein the predetermined capacitance range is between 0.5 nF and 50 nF.

9. The sputtering system of claim 6, further comprising a coaxial cable configured to couple the capacitance tuner with one end of the rotary target.

10. The sputtering system of claim 1, wherein the rotary target includes one or more layers of ceramic materials, and wherein the ceramic materials include one or more of: a transparent conducting oxide (TCO) material and a dielectric material.

11. A sputter deposition method for large-scale fabrication of solar cells, comprising:

placing a plurality of solar cells on a carrier within a reaction chamber;

continuously rotating a rotary target about a longitudinal axis; and

applying an RF power to the rotary target to enable RF sputtering of target material onto surfaces of the solar cells, wherein a length of the rotary target is between 0.5 and 5 meters, and wherein applying the RF power to the rotary target comprises:

dividing the RF power into two portions; and

feeding each of the two portions to an end of the rotary target.

12. The method of claim 11, wherein dividing the RF power into two portions involves dividing the RF power into two equal portions.

13. The method of claim 11, further comprising placing a plurality of magnets inside the rotary target to generate a static magnetic field between the rotary target and a carrier that carries a plurality of solar cells.

14. The method of claim 13, wherein placing the plurality of magnets involves arranging the magnets in such a way that magnetic field is stronger at a location corresponding to an edge of the rotary target, thereby facilitating the magnetic field to have a higher strength at the edge of the rotary target.

15. The method of claim 11, wherein the RF power has an RF frequency of at least 13 MHz.

16. The method of claim 11, further comprising:

coupling a capacitance tuner to one end of the rotary target.

17. The method of claim 16, further comprising periodically tuning the capacitance tuner over a predetermined capacitance range.

18. The method of claim 17, wherein the predetermined capacitance range is between 0.5 nF and 50 nF.

19. The method of claim 16, further comprising inserting a coaxial cable between the capacitance tuner and one end of the rotary target.

20. The method of claim 11, wherein the rotary target includes one or more layers of ceramic materials, and wherein the ceramic materials include one or more of: a transparent conducting oxide (TCO) material and a dielectric material.

* * * * *